Journal of
Mechanical
Science and
Technology

Journal of Mechanical Science and Technology 21 (2007) 1760~1774

Surface tension-affected laminar film condensation problems

Hua Sheng Wang and John W. Rose*

School of Engineering and Materials Science, Queen Mary, University of London, Mile End Road, London, E1 4NS, U. K.

(Manuscript Received May 7, 2007; Revised August 31, 2007; Accepted August 31, 2007)

Abstract

Following Nusselt [1] there were few developments in the theory of laminar film condensation until the advent of digital computers in the 1950s. Approximations used by Nusselt, namely neglect of inertia, convection and surface shear stress (for the free convection case) were then found to give very accurate results for the normal practical range of vapour-to-surface temperature difference. Subsequent developments treated the gas phase and dealt with superheated vapour, condensation in the presence of a non-condensing gas and condensation of mixtures. The temperature discontinuity at the vapour-liquid interface has been studied experimentally and theoretically since the 19th century and more recently in the 1960s by experiments using liquid metals.

In the present paper the focus is on the condensate film and, in particular, the role played by surface tension which is important for condensation on finned surfaces and in microchannels, owing to abrupt changes in curvature of the condensing surface. The way in which surface tension affects condensation heat transfer and difficulties which arise are first illustrated by reference to condensation on a smooth horizontal tube, where the effect of surface tension on heat transfer is minimal. Practically more relevant cases of condensation in microchannels and on finned surfaces and are then discussed and recent results presented.

Keywords: Condensation; Surface tension; Low-fin; Microchannel; Enhanced heat transfer

1. Introduction

In the Nusselt [1] theory the condensate film is treated as a boundary layer for which inertia and convection terms in the momentum and energy balances, as well as the surface shear stress for the free convection case, are neglected. When the properties are taken to be uniform this leads, for natural convection on isothermal surfaces, to

$$\overline{Nu}_L = \frac{\bar{\alpha} L}{k} = \frac{2\sqrt{2}}{3}\left(\frac{Gr_L}{J}\right)^{1/4} \tag{1}$$

for the vertical pate

$$\text{where } J = \frac{k\Delta T}{\mu h_{lg}} \tag{2}$$

*Corresponding author. Tel.: +44 20 7882 5275, Fax.: +44 20 8983 1007
E-mail address: j.w.rose@qmul.ac.uk

$$\text{and } Gr_L = \frac{\rho\Delta\rho g L^3}{\mu^2} \tag{3}$$

and, with the additional assumption that $\delta/R << 1$, to

$$\overline{Nu} = 0.728\ \left(Gr_d/J\right)^{1/4} \tag{4}$$

for the horizontal tube

$$\text{where } Gr_d = \frac{\rho\Delta\rho g d^3}{\mu^2} \tag{5}$$

The Nusselt number is seen to vary as the ¼ power of the Grashof number for both plate and tube as in single-phase natural convection.

In later developments, following the advent of digital computers, the condensate film was treated by various investigators on the basis of the boundary-layer equations and effect of vapour shear stress at the

condensate surface included (see Rose [2]). These analyses led to solutions in the form

$$\frac{Nu}{Nu_{Nu}} = \Phi\left(\frac{c_P \Delta T}{h_{fg}}, \frac{k\Delta T}{\mu h_{fg}}, \frac{\rho\mu}{\rho_v \mu_v} \right) \tag{6}$$

However, for the range of values of $k\Delta T/\mu h_{fg}$ and $c_P \Delta T/h_{fg}$ normally occurring in practice i.e. < 0.01 and < 0.1 respectively, these solutions showed the Nusselt theory to be very satisfactory. Further investigations (see [3], chapter 19 and [4]) treated the case of forced convection, rippling and turbulence in the condensate film as well as the effect of presence of non-condensing gases and condensation of mixtures.

Experimental and theoretical studies of the interface temperature discontinuity have been conducted over more than 100 years and are discussed by Rose [5]. It is now established that this is negligible except for very high condensation rates which may occur when the condensate resistance is small as in the cases of condensation of liquid metals, for the smallest drops in dropwise condensation and in other cases where condensate films are very thin. In these circumstances the temperature drop at the condensate surface may be estimated by

$$\Delta T_i = \zeta\, q \tag{7}$$

where

$$\zeta = \frac{1}{4\xi} \frac{(\gamma+1)}{(\gamma-1)} T_s \sqrt{RT_s} / (v_{fg} / h_{fg}^2) \tag{8}$$

and $\xi = 0.665 \pm 0.003$.

2. Surface tension effects in condensation on a horizontal smooth tube

The varying condensate surface curvature, as the film thickness increases around a tube, in the presence of surface tension gives rise to a tangential pressure gradient in the film

$$\frac{dP}{d\varphi} = \sigma \frac{d}{d\varphi}\left(\frac{1}{r_c}\right) \tag{9}$$

where

$$r_c = \frac{\left\{ \tilde{r}^2 + (d\tilde{r}/d\varphi)^2 \right\}^{3/2}}{\tilde{r}^2 + 2(d\tilde{r}/d\varphi)^2 - \tilde{r} d^2\tilde{r}/d\varphi^2} \tag{10}$$

and $\tilde{r} = R + \delta$.

When this pressure gradient is included in an otherwise Nusselt treatment, the differential equation for the condensate film thickness becomes

$$\frac{d}{d\varphi}\left\{ \Delta^3 \sin\varphi - A\Delta^3 \frac{df}{d\varphi} \right\} = \frac{3B}{\Delta} \tag{11}$$

where

$$f = \frac{(1+\Delta)^2 + 2(d\Delta/d\varphi)^2 - (1+\Delta)\, d^2\Delta/d\varphi^2}{\left\{ (1+\Delta)^2 + (d\Delta/d\varphi)^2 \right\}^{3/2}} \tag{12}$$

$$\Delta = \delta / R \tag{13}$$

$$A = \sigma / \rho g R^2 \tag{14}$$

$$B = \mu k \Delta T / R^3 \rho \Delta \rho g h_{fg} \tag{15}$$

It is readily seen that when gravity dominates over surface tension, i.e. $A \rightarrow 0$, the Nusselt first order equation is recovered. Eq. (11) is fourth order requiring four boundary conditions. Symmetry requires that the first and third derivatives be zero at the top of the tube but otherwise it is not clear how to proceed. It may be noted that the derivation of Eq. (11) requires that $\delta/R << 1$, which does not hold near the bottom of the tube where significant change in condensate surface curvature occurs. The authors are not aware of a wholly satisfactory solution of this problem. This is, however, somewhat academic since near the bottom of the tube where the film become thick, the heat transfer is correspondingly small and has marginal effect on mean heat transfer for the tube as a whole and the surface tension effect is unimportant.

3. Condensation in micro channels

Multi microchannel tubes such as those illustrated in Fig. 1 are becoming increasingly used in air conditioning/refrigeration applications. The typical dimension of a channel is around 1 mm. A wholly theoretical model for the annular or annular-stratified flow regime, which should persist along the channel for some distance from the onset of condensation, has

Fig. 1. Tube sections used by Koyama et al. [16, 17].

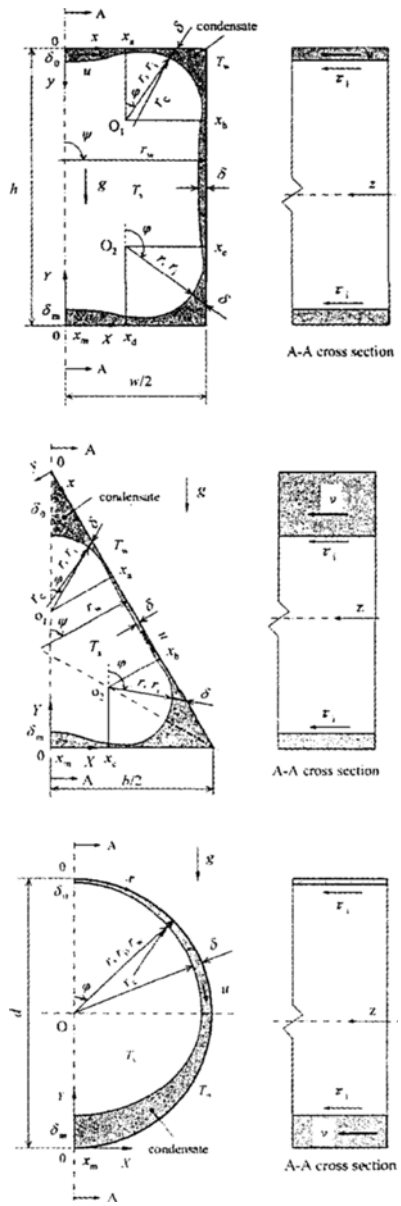

Fig. 2. Model of Wang and Rose [7].

been developed by Wang et al. [6] and described in detail by Wang and Rose [7] (see also [8-15]). The model and coordinate systems for rectangular, triangular and circular section channels are illustrated in Fig. 2. Using the Nusselt approach the momentum conservation equations for flow in the transverse direction, which includes the surface tension term, and in the streamwise direction, which includes the surface shear stress and streamwise pressure gradient, give the velocity profiles in the two directions.

$$u=\frac{1}{\mu}\left[(\rho_l-\rho_v)g\sin\psi+\sigma\frac{\partial}{\partial x}\left(\frac{1}{r_c}\right)\right]\delta^2\left[\left(\frac{y}{\delta}\right)-\frac{1}{2}\left(\frac{y}{\delta}\right)^2\right] \tag{16}$$

$$v=\frac{\tau_i}{\mu}y-\frac{1}{\mu}\left(\frac{dP_v}{dz}\right)\delta^2\left[\left(\frac{y}{\delta}\right)-\frac{1}{2}\left(\frac{y}{\delta}\right)^2\right] \tag{17}$$

Conservation of mass, that is, equating increase in mass flow in both streamwise and transverse directions across an element (control region) of the film to the condensation rate on its surface gives the differential equation for the condensate film thickness

$$\frac{(\rho_l-\rho_v)g}{3\nu}\frac{\partial}{\partial x}(\delta^3\sin\psi)+\frac{\sigma}{3\nu}\frac{\partial}{\partial x}\left\{\delta^3\frac{\partial}{\partial x}\left(\frac{1}{r_c}\right)\right\}+\frac{1}{2\nu}\frac{\partial\left(\tau_i\delta^2\right)}{\partial z}-\frac{(\rho_l-\rho_v)g}{3\nu}\frac{\partial}{\partial z}\left(\delta^3\right)-\frac{1}{3\nu}\frac{\partial}{\partial z}\left(\delta^3\frac{dP_v}{dz}\right)=\frac{1}{(1+\zeta\ k/\delta)}\frac{k(T_s-T_w)}{h_{fg}\delta} \tag{18}$$

where $$\frac{1}{r_c}=\frac{\partial^2\delta/\partial x^2}{\left\{1+(\partial\delta/\partial x)^2\right\}^{3/2}} \tag{19}$$

using Cartesian coordinates which rotate at corners, with x measured along the channel wall from the top point of symmetry, when considering channel sides, and

$$\frac{(\rho_l-\rho_v)g}{3\nu}\frac{\partial}{r\partial\varphi}\left[\delta f_\varphi(\delta)\ \sin\varphi\right]+\frac{\sigma}{3\nu}\frac{\partial}{r\partial\varphi}\left[\delta f_\varphi(\delta)\frac{\partial}{r\partial\varphi}\left(\frac{1}{r_c}\right)\right]+\frac{1}{\nu}\frac{\partial}{\partial z}\left[\delta f_\tau(\delta)\ \tau_i\right]-\frac{(\rho_l-\rho_v)g}{4\nu}\frac{\partial}{\partial z}\left[\delta f_z(z)\right]$$

$$+\frac{1}{4\nu}\frac{\partial}{\partial z}\left[\delta f_z(\delta)\ \frac{\mathrm{d}P_v}{\mathrm{d}z}\right] = \frac{1}{1+\dfrac{\zeta\ k}{r_w \ln\left[r_w/(r_w-\delta)\right]}}\ \frac{k(T_s-T_w)}{h_{fg} r_w \ln\left[r_w/(r_w-\delta)\right]} \tag{20}$$

$$\frac{1}{r_c} = \frac{r_i^2 + 2(\partial r_i/\partial\varphi)^2 - r_i\left(\partial^2 r_i/\partial\varphi^2\right)}{\left\{r_i^2 + (\partial r_i/\partial\varphi)^2\right\}^{3/2}} \tag{21}$$

using polar coordinates when considering corners and for a circular section channel. The functions f_φ, f_τ, f_z are defined in Wang and Rose [7].

For completeness, and because it was thought that this may be significant at the high condensation fluxes where the condensate film is very thin, the interface temperature drop [see Eq. (7)] has been included in the term on the right-hand side of Eqs. (18) and (20). It may be noted that Eqs. (18) and (20) are valid to the same extent as the Nusselt theory but uncertainty will arise in the micro channel case when solving since this requires estimates for surface shear stress and streamwise pressure gradient.

It is seen that Eqs. (18) and (20) are fourth order in x and φ and we might anticipate problems in specifying sufficient boundary conditions as in the horizontal tube problem. However, for rectangular and equilateral triangular channels *with a horizontal side* and for a circular channel, there is a central vertical plane about which the condensate film profile is symmetrical, so that the first and third derivatives are zero at the centre of the top and bottom of the channel giving the required four boundary conditions. It is not clear, however, how the problem should be treated in general, say for a *tilted* rectangular or triangular channel. In the flow direction the required boundary condition is given by the fact that the film thickness is zero for the whole perimeter at the location where condensation commences.

Eqs. (18) and (20) have been solved numerically for various cases using preliminary estimates of the local shear stress at the condensate surface estimated as for single-phase flow, based on the method of Churchill [18], modified to account for "suction" due to condensation (see [7]).

Specimen results shown in Figs. 3-9 are for saturated R134a vapour for a given inlet condition and flow rate and specified uniform channel surface temperature which is less than that of the vapour so that condensation commences at the inlet. Fig. 3 shows calculated condensate film profiles at different

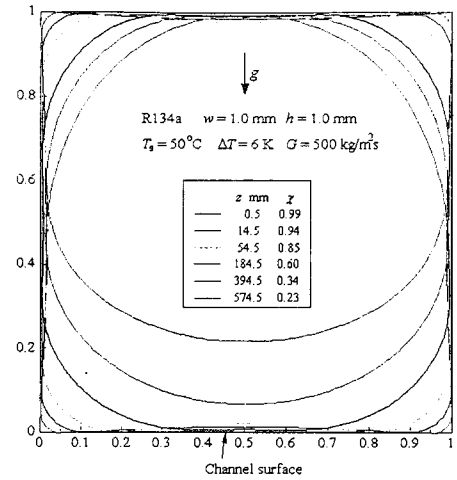

Fig. 3. Development of condensate film profiles along a horizontal 1 mm square channel [7].

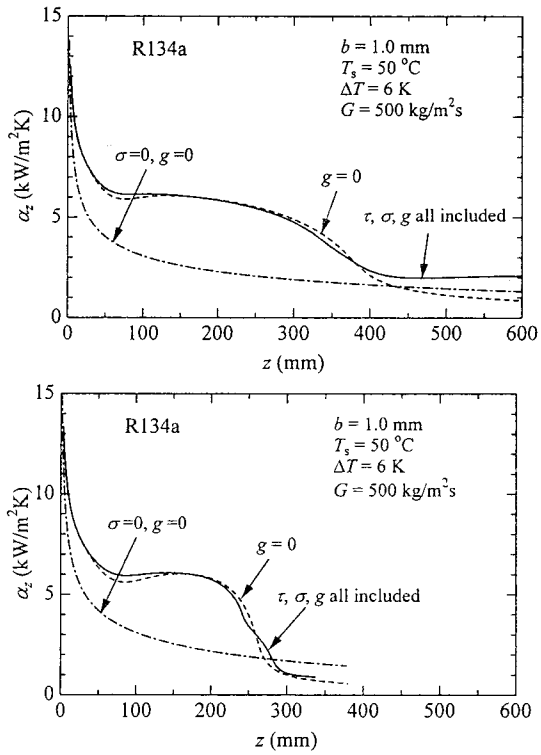

Fig. 4. Specimen calculations of variation along a channel of the mean heat-transfer coefficient for horizontal 1 mm square channel (upper figure) and triangular channel with side 1 mm (lower figure) [7].

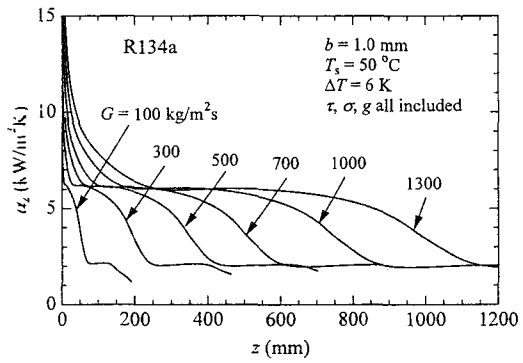

Fig. 5. Specimen calculations of variation along a channel of the mean heat-transfer coefficient for a horizontal 1 mm square channel for different vapour mass fluxes (mass velocities) [7].

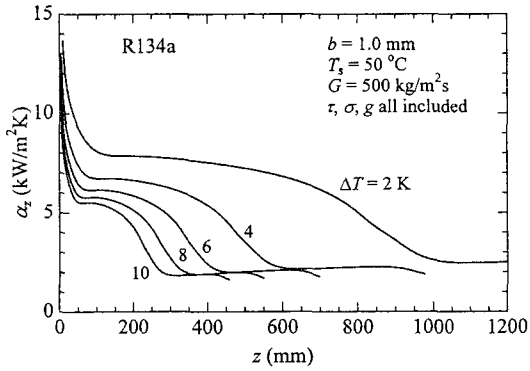

Fig. 6. Specimen calculations of variation along a channel of the mean heat-transfer coefficient for a horizontal 1 mm square channel for different vapour-to-surface temperature differences [7].

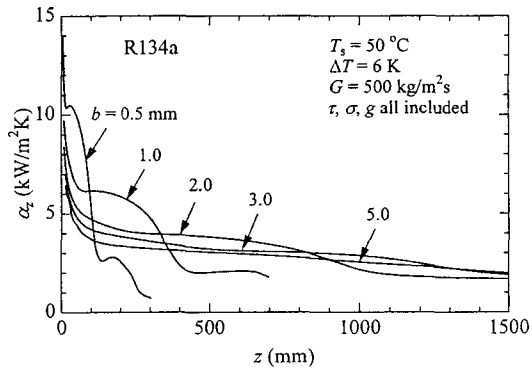

Fig. 7. Specimen calculations of variation along a channel of the mean heat-transfer coefficient for a horizontal square channel for different channel sizes [7].

distances along a horizontal 1 mm square section channel. Extremely thin films are seen in the vicinity of change in condensate surface curvature. This is most evident near the inlet. It is interesting to note that, for the square channel, the film remains thin along a significant part of the upper surface at appreciable distances along the channel where the lower part becomes filled with condensate due to gravity.

For the same conditions Fig. 4 shows the dependence of circumferential mean heat-transfer coefficient α_z on distance along the triangular and square channels. The effects on the results of omitting surface tension and gravity terms are also illustrated. As in the case of the simple Nusselt theory the high heat-transfer coefficient at the inlet results from imposing a temperature difference between wall and vapour at the onset of condensation. After the initial high values the coefficient remains almost constant until, when condensate in the corners occupies a substantial part of the channel (see Fig. 3), it falls more steeply, particularly for the triangular channel. The enhancing effect of surface tension over the first 250 to 350 mm in this case is clearly seen, approximately doubling the heat-transfer coefficient over that part of the channel for both square and triangular channels. The effect of gravity is essentially negligible in this region. The importance of gravity at further distances along the channel is much more significant for the square section channel, approximately doubling the heat-transfer coefficient, due to the thinning of the film on the upper surface mentioned earlier earlier and seen in Fig. 3. For the triangular channel gravity continues to have small effect at further distances along the channel.

Fig. 5 shows the variation of circumferential mean heat-transfer coefficient with distance along the channel for different mass fluxes. It is seen that the enhancing effect of surface tension takes place over a longer distance of the channel for higher mass flux. It is interesting to note that the values over the horizontal portions of the curves are almost the same for all mass fluxes, suggesting perhaps that the effect of surface tension is the dominating mechanism for that part of the channel.

Fig. 6 shows the effect of vapor-to-surface temperature difference. It is seen that the heat-transfer coefficient is higher and for a longer distance along the channel for lower vapour-to-surface temperature difference reflecting lower condensation rates and

correspondingly thinner condensate films. At higher values of ΔT the coefficient is lower and falls off more steeply as the channel becomes more rapidly filled with condensate at the correspondingly higher condensation rates.

Fig. 7 shows the effect of channel size for a square section horizontal microchannel. Heat-transfer coefficients are shown for square channels having side of 0.5, 1.0, 2.0, 3.0 and 5.0 mm. The enhancing effect of surface tension near the entry part of the channel is higher for the smaller channels but falls off more rapidly along the channel. The smaller channels become more rapidly "flooded" with condensate so that the heat-transfer coefficient further along the channel is significantly lower than for the larger channels. For the larger channels with side 3 and 5 mm there is little, if any, discernable effect of surface tension enhancement.

Fig. 8 shows results for different channel shapes. It is seen that all shapes outperform the circular section towards the channel inlet but, as expected, the heat-transfer coefficient for non-circular channels, which condense more vapour in the initial part of the channel, subsequently fall below that of the circular channel.

Fig. 9 shows results for a square-section channel for different channel inclinations. It is seen that for the sections of channel where surface tension dominates the heat-transfer coefficient is essentially independent of inclination.

Fig. 10 shows results for condensation of R152a, R134a, R22, R410A, propane, ammonia and carbon dioxide in a 1mm square section microchannel (see [19]). For the given conditions ammonia is the best performing fluid and carbon dioxide the worst. The results reflect the respective values of thermal conductivity, latent heat and surface tension.

Preliminary calculations have also been made (see [17]) for comparison with the experimental data reported by Koyama et al. [16, 17] for the upper tube in Fig. 1 (channel width 1.36 mm, height 1.03 mm) with vapour inlet pressure 1.70 MPa and three vapour mass fluxes (mass velocities). Differences between theory and measurement may in part be attributable to uncertainty in the interpretation of the experimental results as described by Wang and Rose [15]). As may be seen from Fig. 11 agreement is encouraging but further comparisons are needed before firm conclusions can be drawn.

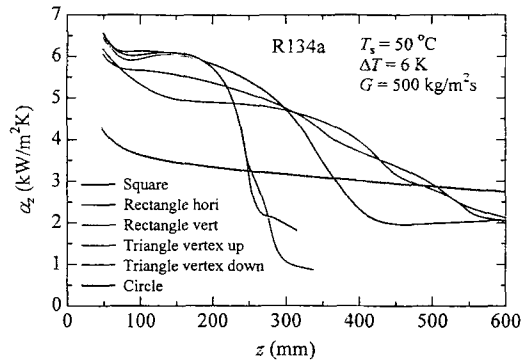

Fig. 8. Specimen calculations of variation along a horizontal channel of the mean heat-transfer coefficient for various channel shapes - square side 1 mm, rectangle 1 mm x 1.5 mm, triangle side 1 mm, circle diameter 1 mm [15].

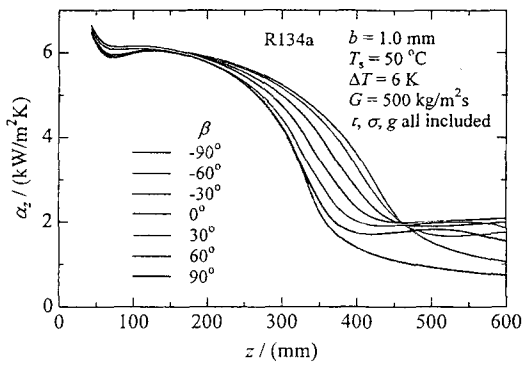

Fig. 9. Variation of mean (over perimeter of channel) heat-transfer coefficient with distance for various channel inclinations for square section channel [13].

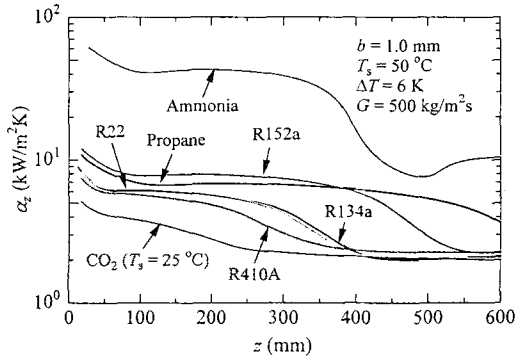

Fig. 10. Variation of mean (over perimeter of channel) heat-transfer coefficient with distance for various fluids for a horizontal 1 mm square channel [19].

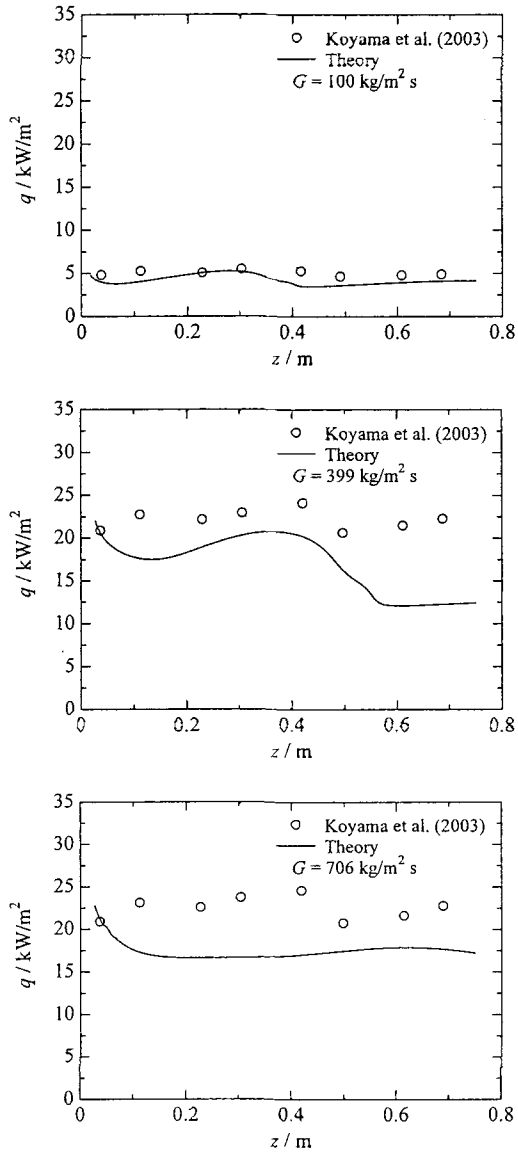

Fig. 11. Measured and calculated heat flux distributions along the channel for R134a [14].

4. Condensation on low-finned tubes

Fig. 12 shows a typical low-finned tube. The earliest model for this problem is that of Beatty and Katz [20] who treated the fin flanks and interfin tube surface on the basis of the Nusselt theory for plane surfaces and horizontal tubes respectively. Normalization of the mean heat flux or heat-transfer coefficient by the smooth-tube Nusselt result gave an *enhancement ratio* dependant only on the geometry i.e. same for all fluids. This appeared to give satisfactory results for some low surface tension fluids and available geometries at that time.

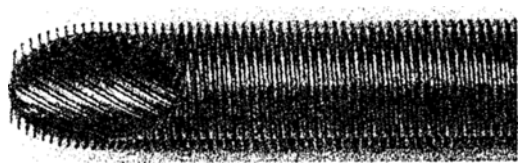

Fig. 12. Low-finned tube (Wieland Werke, Gewa -KS).

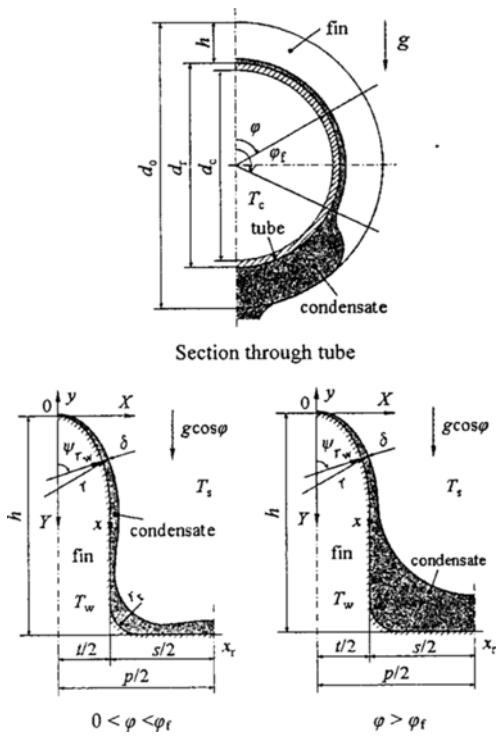

Fig. 13. Condensation on low-finned tube. Physical model and coordinates.

More recently attempts have been made to solve this problem which include surface tension effects. Here surface tension plays a crucial role and, not surprisingly in view of what has been said above regarding smooth tubes, significant difficulties are encountered. Honda and Nozu [21] and Honda et al. [22] have given approximate and partial solutions. A theoretically-based correlation has been given by Rose [23]. The most recent theoretical investigation of Wang and Rose [24] is outlined below.

Fig. 13 illustrates film condensation on a low-finned tube with arbitrary fin profile. The orthogonal coordinates X, Y have origin at the centre of the fin tip, x is measured along the fin surface from the centre of

the fin tip, y is measured normally outward from the fin surface. φ is measured circumferentially from the top of the tube. d_o and d_r are the tube diameters at fin tip and root respectively. h is the fin height. t and s are fin thickness and spacing at the fin root, respectively.

As observed in practice, and illustrated in Fig. 13, the condensate film between fins thickens abruptly at some position around the tube, referred to as the *flooding* or *retention angle* φ. The condensate profile where the film is relatively thick (i.e. at the fin root and in the lower so-called *flooded* region) is close to that found under non-condensing or *static* conditions where the surface is wetted and liquid is retained by the balance between surface tension and gravity (see [25]). A correct solution of the condensation problem should approach the static retained liquid profile as the condensation rate approaches zero. Earlier partial solutions do not predict "flooding".

When the surface tension-induced pressure gradient is included in an otherwise Nusselt treatment, conservation of mass, momentum and energy yields (see [19]) the differential equation for local film thickness δ

$$\frac{(\rho_l-\rho_v)g\cos\varphi}{3\nu}\frac{\partial}{\partial x}\left(\delta^3\sin\psi\right)-\frac{\sigma}{3\nu}\frac{\partial}{\partial x}\left\{\frac{\partial}{\partial x}\left(\frac{1}{r_x}+\frac{1}{r_\varphi}\right)\delta^3\right\}$$
$$+\frac{2(\rho_l-\rho_v)g\cos\psi}{3\nu d_o}\frac{\partial}{\partial\varphi}\left(\delta^3\sin\varphi\right)-\frac{4\sigma}{3\nu d_o^2}\frac{\partial}{\partial\varphi}\left\{\frac{\partial}{\partial\varphi}\left(\frac{1}{r_x}+\frac{1}{r_\varphi}\right)\delta^3\right\}$$
$$=\frac{1}{(1+\zeta\ k/\delta)}\frac{k\ (T_s-T_w)}{h_{fg}\delta} \tag{22}$$

where ψ is the angle of the normal to the fin surface to the Y coordinate (see Fig. 13), and r_x and r_φ are the local radii of the curvature of the condensate surface in the fin cross-section and tube cross-section, respectively, given by

$$\frac{1}{r_x}=\frac{\frac{1}{r_w}+\left(\frac{2}{r_w^2}+\frac{\delta}{r_w^3}\right)\delta+\left(\frac{2}{r_w}\frac{\partial\delta}{\partial x}-\frac{\delta}{r_w^2}\frac{dr_w}{dx}\right)\frac{\partial\delta}{\partial x}-\left(1+\frac{\delta}{r_w}\right)\frac{\partial^2\delta}{\partial x^2}}{\left[\left(1+\frac{\delta}{r_w}\right)^2+\left(\frac{\partial\delta}{\partial x}\right)^2\right]^{3/2}} \tag{23}$$

$$\frac{1}{r_\varphi}=\frac{\left(\frac{d_t}{2}+h-Y_w+\delta\cos\psi\right)^2+2\left(\frac{\partial\delta}{\partial\varphi}\cos\psi\right)^2-\left(\frac{d_t}{2}+h-Y_w+\delta\cos\psi\right)\frac{\partial^2\delta}{\partial\varphi^2}\cos\psi}{\left[\left(\frac{d_t}{2}+h-Y_w+\delta\cos\psi\right)^2+\left(\frac{\partial\delta}{\partial\varphi}\cos\psi\right)^2\right]^{3/2}} \tag{24}$$

where r_w is the radius of the curvature of the fin surface and Y_w is the Y-coordinate of the fin surface.

Eq. (22) is the fourth order in both x and φ. From symmetry boundary conditions are

$$\partial\delta/\partial x=\partial^3\delta/\partial x^3=0 \text{ at } x=0 \text{ and } x_r \text{ (centre of interfin space)} \tag{25}$$

$$\partial\delta/\partial\varphi=\partial^3\delta/\partial\varphi^3=0 \text{ at } \varphi=0 \text{ (top of tube)} \tag{26}$$

As in the case of the smooth tube when surface tension is included, two further φ-direction boundary conditions are needed. Honda and Nozu [21] omitted all φ derivatives in Eq. (22) as well as the curvature in the circumferential direction in the second term and used a somewhat arbitrary boundary condition for the slope of the condensate film near the fin root. Honda et al. [22] later included the third term in Eq. (22) with a first derivative with respect to φ. These solutions do not show the abrupt thickening of the film.

The most recent approach by Wang and Rose [19], based on the original approach of Honda and Nozu [21] and Honda et al. [22] also neglects the φ - direction curvature in the second term of Eq. (22) as well as the whole of the fourth term involving φ - direction derivates. When the fourth term in Eq. (22) is omitted, the solution as noted above, does not predict the abrupt thickening of the condensate film at the retention angle. The effect of omitting the fourth term in Eq. (22) is effectively accounted for by Wang and Rose [24] by ensuring that solutions of the differential equation for the unflooded parts of the

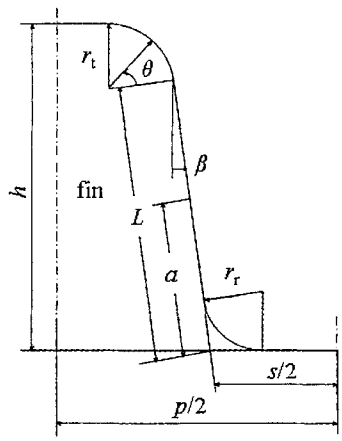

Fig. 14. Nomenclature used in static configuration equations.

surfaces blend smoothly with the statically-retained configuration for the part of the tube below the retention angle, the latter determined on the basis of the approach of Masuda and Rose [25]. This should not cause appreciable error since condensation and heat transfer below the retention angle are very small except at the fin tip. The interfin space for the region below the retention angle is treated on the basis of static retention and provides the required end condition to solve for δ along the fin tip in the flooded part of the tube.

The static configuration of retained liquid on a wetted tube is obtained by equating the pressure drop across the meniscus to that for a vertical column of liquid with height equal to the vertical distance from the location in question to the bottom of the tube. For low fins ($h/R << 1$) and when $r_x << r_\varphi$, this gives

$$\cos\varphi = \sigma / (r_x R \rho g) - 1 \tag{27}$$

Above the retention position and referring to Fig. 14, the meniscus touches the fin flank and the interfin tube surface and has radius

$$r_x = \frac{a\cos\beta}{1-\sin\beta} \tag{28}$$

For the usual geometry where $L > s/2$, "flooding" commences when the menisci on adjacent fins meet at the centre of the interfin space and $a = s/2$. Since the meniscus is tangential to both flank and tube surface geometry gives

$$r_x = \frac{s\cos\beta}{2(1-\sin\beta)} \tag{29}$$

and the retention angle φ_f may be found from Eq. (27).

For $\varphi > \varphi_f$ the meniscus rises rapidly up the fin flanks, where the meniscus touches the fin flank and is symmetrical about the centre of the interfin space so that

$$r_x = \frac{s}{2\cos\beta} + a\tan\beta \tag{30}$$

with the corresponding angle φ obtained from Eq. (27). Eq. (30) holds while $s/2 \le a \le L$.

For larger values of φ, when the meniscus touches the curved part of the meniscus, the radius of curvature is given by

$$r_x = \frac{s/2 + L\sin\beta + r_t\cos\beta}{\cos(\theta+\beta)} - r_t \tag{31}$$

and the corresponding angle φ is again obtained from Eq. (27).

Fig. 15 shows specimen dimensionless static retention profiles for water on a finned tube with dimensions given in the figure. It is seen that for this case flooding commences at an angle of 73.3° from the top of the tube and the meniscus reaches the tip of the fin at an angle of 79.2°. The meniscus in the interfin space rises with angle becoming almost horizontal at an angle of 170.2 °. Fig. 16 shows the film thickness at the centre of the interfin space for three fin spacings and otherwise the same geometry as in Fig. 15. For spacing between fins of 1.0 mm and 1.5 mm there is no statically retained liquid on the surface at the centre of the interfin surface up to angles of around 73 ° and 102 ° respectively. For larger angles the retained liquid thickness at the centre of the interfin space increases rapidly where the meniscus touches the straight side of the fin (green in Fig. 16) and more slowly thereafter when the meniscus touches the curved edge of the fin tip (blue in Fig. 16). When the spacing between fins is 0.5 mm the meniscus already touches the curved edges of the fin tip at the top of the tube.

Fig. 17 shows calculated film surface profiles over the whole of the fin surface during condensation. Solutions above the flooding angle were obtained by solving Eq. (22) neglecting terms as described above. When the solution is continued towards the bottom of the tube flooding is not predicted owing to omission of φ-derivates. For the lower part of the tube results were obtained along the fin tip by forcing the solution of Eq. (22) to blend with the static profile below the flooding angle. It is seen that the film is relatively thick towards the centre of the fin tip. This is due to the relatively high pressure near the edge of the tip where the surface curvature is largest and the fact that the pressure gradient due to surface tension directs condensate towards the centre of the fin tip as well as radially inward along the fin flank. The film is very thin near the fin tip and along the fin flank above the retention angle. Fig. 18 shows, for the same case, the variation of film thickness with distance along the fin surface from the centre of the fin tip. It is again seen that the film becomes relatively thick at the centre of the fin tip. Very thin film regions are seen where x/p lies approximately between 0.17 and 0.5

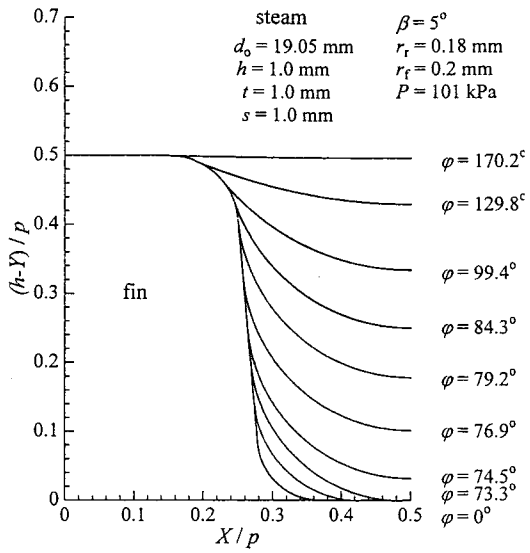

Fig. 15. Specimen dimensionless static liquid (water) film profiles along the fin surface at different angles (symbols are defined in Fig. 1 and text; red: 0 < φ < 73.3°, green: 73.3° < φ < 79.2°, blue: 79.2° <φ < 170.2°).

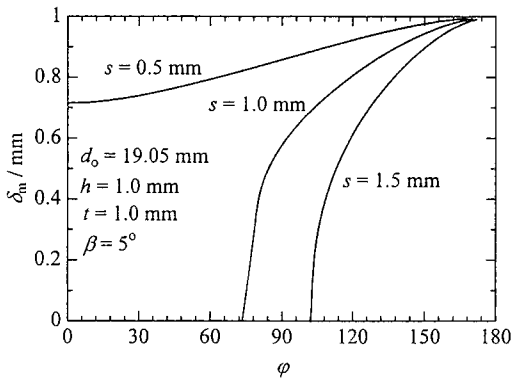

Fig. 16. Static retention: Specimen film thicknesses for water at the centre of interfin space, (green: 73.3° <φ < 79.2°, blue: 79.2° <φ < 170.2°).

(Note that $x/p \approx 0.9$ corresponds to the centre of the interfin space for this geometry). Fig. 19 shows the corresponding heat flux distribution over the fin surface. The regions of high heat flux correspond to those of small fin thickness in Fig. 18.

5. Theoretically-based correlation

Pending complete solution of this problem a correlation by Rose [23] provides a practical and simple method of evaluating heat-transfer coefficients for condensation on low finned tubes. In this approach,

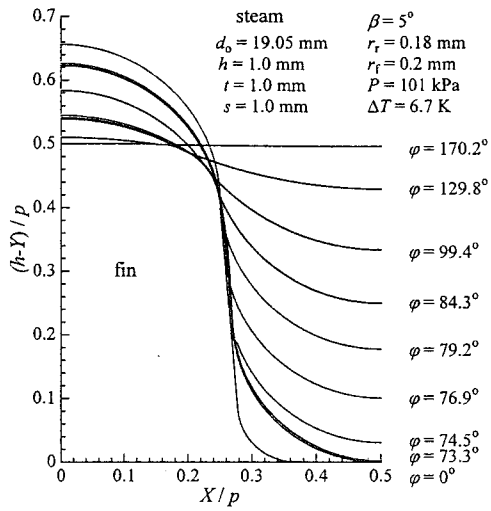

Fig. 17. Specimen dimensionless condensate distributions along the fin surface at different angles (red: 0 <φ < 73.3°, green: 73.3° <φ < 79.2°, blue: 79.2° <φ < 170.2°).

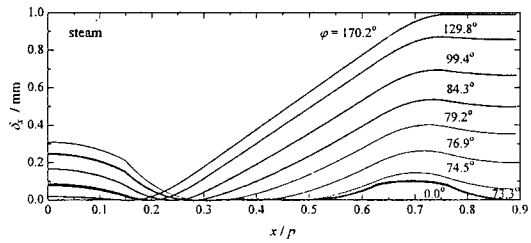

Fig. 18. Specimen results for condensate film profiles on the fin surface at different angles (red: 0 <φ < 73.3°, green: 73.3° <φ < 79.2°, blue: 79.2° <φ < 170.2°).

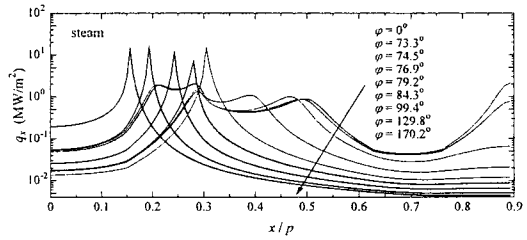

Fig. 19. Specimen results for heat flux profiles on the fin surface at different angles (red: 0 <φ < 73.3°, green: 73.3° <φ < 79.2°, blue: 79.2° <φ < 170.2°).

outlined below, static retention is used to determine those parts of the fin and tube surfaces which are not effectively blanked by retained liquid. For the unblanked parts of the fin flanks and interfin tube surface and for the fin tip over the whole of the tube surface, a combination of the appropriate Nusselt equation with an expression based on dimensional

analysis for the surface tension effect was used to determine the heat-transfer rate. The form of expression used was such that the heat flux (based on the smooth tube area) varied as the ¾ power of the temperature difference, as in the Nusselt theory and found by experiment for low-finned tubes. Two disposable constants were found by fitting accurate data for fluids with widely different properties. The final result is in the form of an algebraic expression for the *enhancement ratio* (ratio of heat flux or heat-transfer coefficient for finned tube based on smooth tube area divided by that for a smooth tube with the same diameter and for the same vapour-to-surface temperature difference) which is independent of temperature difference or heat flux:

$$\varepsilon_{\Delta T} = \frac{d_0}{d_r}\frac{t}{(b+t)}T_r + \frac{\varphi}{\pi}\frac{(1-f_f)}{\cos\beta}\left(\frac{d_o^2-d_r^2}{2d_r(b+t)}\right)T_f$$
$$+2.96\frac{\varphi}{\pi}(1-f_s)\frac{s}{(b+t)}T_s \quad (32)$$

where

$$f_f = \frac{1-\tan(\beta/2)}{1+\tan(\beta/2)} \cdot \frac{2\sigma\cos\beta}{\rho g d_r h} \cdot \frac{\tan(\varphi/2)}{\varphi} \quad (33)$$

$$f_s = \frac{1-\tan(\beta/2)}{1+\tan(\beta/2)} \cdot \frac{4\sigma}{\rho g d_r s} \cdot \frac{\tan(\varphi/2)}{\varphi} \quad (34)$$

$$T_t = \left\{\frac{d_r}{d_o} + 0.509\frac{\sigma d_r}{\Delta\rho g t^3}\right\}^{1/4} \quad (35)$$

$$T_f = \left\{2.815\frac{d_r}{h_v} + 0.509\frac{\sigma d_r}{\Delta\rho g h^3}\right\}^{1/4} \quad (36)$$

$$T_s = \left\{3.56\{\xi(\varphi)\}^3 + 0.509\frac{\sigma d_r}{\Delta\rho g s^3}\right\}^{1/4} \quad (37)$$

$$h_v = h\varphi/\sin\varphi \quad \text{for } \varphi \le \pi/2$$
$$h_v = h\varphi/(2-\sin\varphi) \text{ for } \varphi \ge \pi/2 \quad (38)$$

$$\xi(\theta) = \frac{1}{2^{1/3}\theta^{4/3}}\left[\int_0^\theta \left\{\frac{\int_0^\theta (\sin\theta)^{1/3}\,d\theta}{(\sin\theta)^{4/3}}\right\}^{-1/4} d\theta\right]^{4/3} \quad (39)$$

which may be approximated by

$$\xi(\theta) = 0.874 + 0.1991\times10^{-2}\theta - 0.2642\times10^{-1}\theta^2$$
$$+0.553\times10^{-2}\theta^3 - 0.1363\times10^{-2}\theta^4 \quad (40)$$

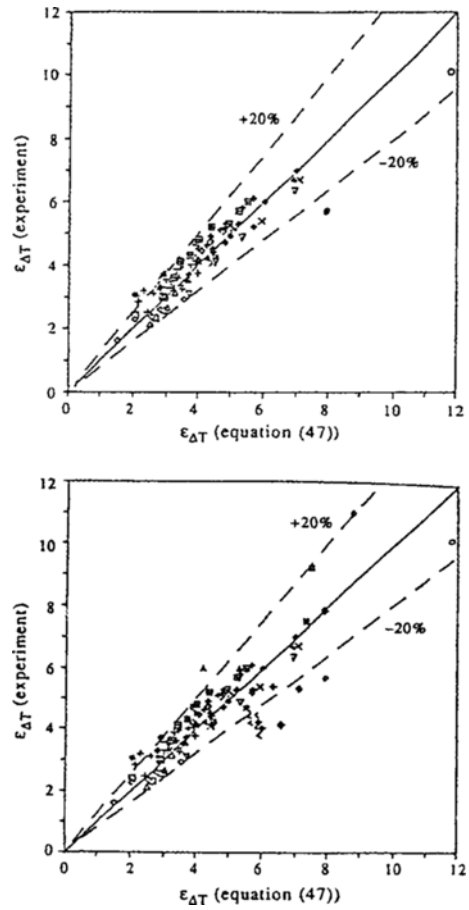

Fig. 20. Experimental versus calculated values of enhancement ratio [23].

As may be seen from Eqs. 32 - 40 $\varepsilon_{\Delta T}$ depends only on the property ratio σ/ρ, gravity and geometry. To determine the mean heat-transfer coefficient (based on the smooth tube area) one simply calculates the Nusselt value for the given ΔT and multiplies by $\varepsilon_{\Delta T}$ given by Eq. (32). Comparisons with data are shown in Figs. 20-24. Fig. 20 compares calculated and measured enhancement ratios. Comparisons of this type can hide incorrect dependence on individual parameters. Figs. 21-24 show that the expression gives the correct dependence on fluid properties and the geometric parameters.

The above results all apply to quiescent vapour. Cavallini et al. [29] fitted data for high velocity vapour to their data for refrigerants using a correlation which satisfied the above result in the low velocity limit. The correlation fits most of the heat-transfer coefficient data for several fluids (excluding steam) to within about 25% as shown in Fig. 25. However, the

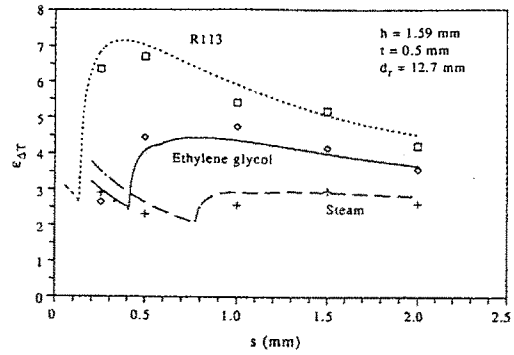

Fig. 21. Dependence of enhancement ratio on spacing between fins [23].

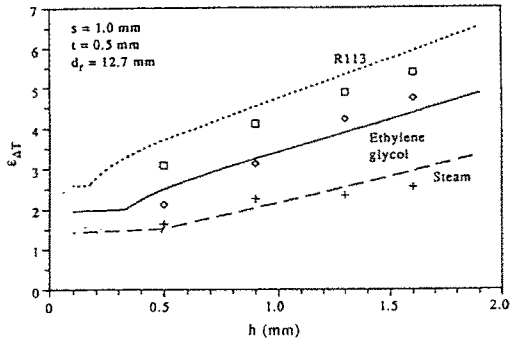

Fig. 22. Dependence of enhancement ratio on spacing between fins [23].

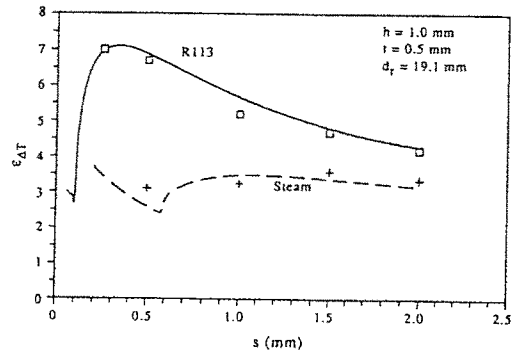

Fig. 23. Comparisons of correlation with data for larger diameter tube [23].

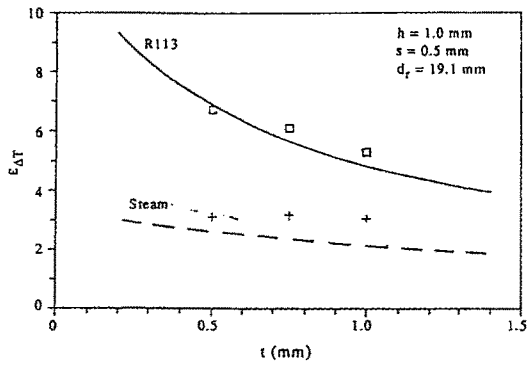

Fig. 24. Dependence of enhancement ratio on fin thickness [23].

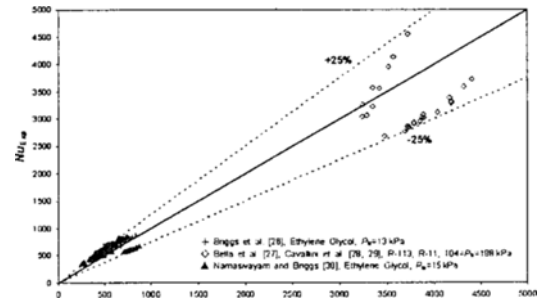

Fig. 25. Forced convection condensation on low-finned tubes: comparison of correlation of Cavallini et al. [4] with data for several fluids [35].

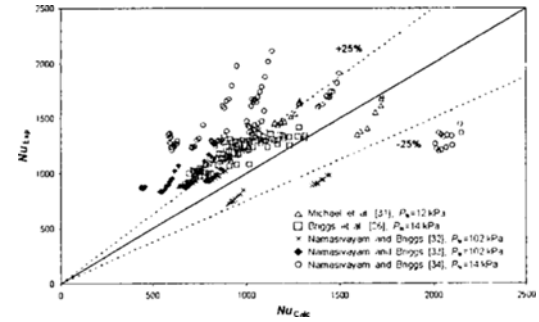

Fig. 26. Forced convection condensation on low-finned tubes: comparison of correlation of Cavallini et al. [4] with data for steam [35].

correlation does not agree well with data for steam as shown in Fig. 26.

6. Concluding remarks

When account is taken of the pressure drop across the vapour-condensate interface, in an otherwise Nusselt approach to condensation heat transfer, it is not always possible to supply sufficient boundary conditions. For the case of the horizontal tube the rate of change of curvature of the surface of the condensate film is only significant very close to the lowermost part of the tube where the assumption that the film is thin also becomes invalid. However, since the heat transfer through the relatively thick film is small the Nusselt solution for the tube as a whole is satisfactory.

For condensation in channels where there exist two

positions of symmetry in the cross section at the top and bottom (triangular and rectangular sections with a horizontal side and a circular channel) the required four boundary conditions can be specified and solutions obtained. While the differential equation and boundary conditions in this case have the same validity as the simple Nusselt theory, solutions require estimates of the streamwise surface shear stress and pressure gradient. Furthermore solutions are only valid so long as the Nusselt conditions prevail, in particular while the condensate surface is smooth and the flow regime is annular or annular/stratified.

Condensation on finned surfaces presents greater difficulty. No wholly satisfactory or complete theoretical solution has yet been obtained. The problem is still under investigation and improved solutions are awaited. An earlier theoretically-based correlation has the advantage of simplicity and agrees well with experimental data for quiescent vapour but so far no satisfactory extension of this to cover higher vapour velocities and having validity over a wide range of fluid properties is available.

Nomenclature

A : Defined in Eq. (14)
B : Defined in Eq. (15)
b : Spacing between fin flanks at fin tip
c_P : Isobaric specific heat capacity of vapour
c_v : Isochoric specific heat capacity of vapour
b : Width of plate, side of channel
d : Diameter of tube
d_o : Diameter at fin tip
d_t : Diameter at fin tip
d_r : Diameter at fin root
f : Defined in Eq. (12)
f_f : Defined in Eq. (33)
f_s : Defined in Eq. (34)
G : Mass flux (mass velocity)
Gr_L : Grashof number based on plate height {see Eq. (3)}
Gr_d : Grashof number based on tube diameter {see Eq. (5)}
h : Fin height
h_v : Defined in Eqs. (38)
h_{fg} : Specific latent heat of evaporation
J : Defined in Eq.(2)
k : Thermal conductivity of condensate
L : Height of plate, distance along fin flank (see Fig. 14)
m : Local condensation mass flux
m_x : Condensation mass flow per length normal to flow direction
m_z : Condensation mass flow per length normal to flow direction
Nu_L : Mean Nusselt number for a plate of height L
Nu : Mean Nusselt number for horizontal tube
P : Pressure in condensate film
P_v : Pressure in vapour
p : Fin pitch
q_x : Local heat flux
q : Mean heat flux
R : Specific ideal gas constant, radius of tube
r_c : Radius of curvature of condensate surface
$\tilde{r}$: $R + \delta$
r_x : Radius of curvature in fin cross section
r_w : See Fig. 2
r_r : Radius at fin root (see Figs. 13, 14)
r_φ : Radius of curvature in tube cross section
s : Space between fins at root, see Figs. 13, 14
T_s : Saturation temperature
T_w : Surface temperature
T_f : Defined in Eq. (36)
T_s : Defined in Eq. (37)
T_t : D efined in Eq. (35)
t : Fin thickness at tip
u : Velocity in condensate film in x-direction
v : Velocity in condensate film in z-direction
v_f : Specific volume of saturated liquid
v_g : Specific volume of saturated vapour
v_{fg} : $v_g - v_f$
x : Distance along surface (see Figs. 12, 13)
y : Distance normal to surface (see Fig. 2)
z : Distance along channel (see Fig. 2)
α : Heat-transfer coefficient
$\bar{\alpha}$: Mean heat-transfer coefficient
α_z : Local circumferential mean heat-transfer coefficient at distance z along channel
β : Angle between fin flank and radial plane (see Fig. 14), inclination of channel to horizontal
γ : c_P / c_v
Δ : δ/R
$\Delta\rho$: $\rho - \rho_v$
δ : Condensate film thickness measured normally to condensing surface
$\varepsilon_{\Delta T}$: Enhancement ratio (vapour-side heat-transfer coefficient for finned tube based on smooth tube area divided by value for smooth tube for the same temperature

difference)

ζ : Defined in Eq. (8)

μ : Viscosity of condensate

ν : Kinematic viscosity of condensate

ρ : Density of condensate

ρ_v : Density of vapour

τ_i : Streamwise shear stress on condensate surface in channel

φ : Angle from top of tube, angle defined in Fig. 2

Acknowledgments

This work was supported by the Engineering and Physical Sciences Research Council (EPSRC) of the UK through grants GR/S20345/1, EP/C510925/1 and EP/D500133/1.

References

[1] W. Nusselt, Die oberflachenkondensation des wasserdampfes, *Z. Ver. Dt. Ing.* 60 (1916) 541-546, 569-575.

[2] J. W. Rose, Fundamentals of condensation heat transfer: laminar film condensation, *JSME Int. Journal*. 31 (2) (1988) 357-375.

[3] Handbook of Phase Change, Eds. S. G. Kandlikar, M. Shoji and V. K. Dhir, Taylor and Francis, Chapter 19, Film Condensation, (1999) 523-580.

[4] T. Fujii, Theory of laminar film condensation, Springer-Verlag. (1991).

[5] J. W. Rose, Interphase matter transfer, the condensation coefficient and dropwise condensation, *Proc. 11th Int. Heat Transfer Conf.* Kyongju, Korea, (1998) 89-104.

[6] H. S. Wang, J. W. Rose and H. Honda, A theoretical model of film condensation in square section microchannels, *Trans. IChemE, Chem. Eng. Research and Design*. 82 (2004) 430-434.

[7] H. S. Wang and J. W. Rose, A theoretical model for condensation in microchannels, *Trans. ASME J. Heat Transfer*. 127 (2005) 1096-1105.

[8] H. S. Wang and J. W. Rose, Condensation in microchannels, *Proc. 6th Int. Symp. on Heat Transfer*. Beijing, China, (2004) 22-31.

[9] H. S. Wang and J. W. Rose, Film condensation in horizontal triangular section microchannels, Proc. *2nd Int. Conf. on Microchannels and Minichannels*, ASME Rochester, New York, (2004) 661-666.

[10] H. S. Wang and J. W. Rose, Film condensation in horizontal microchannels: effect of channel shape, *Proc. 3rd Int. Conf. Microchannels and Minichannels*, ASME Toronto, CD, paper ICMM 2005-75260. (2005).

[11] H. S. Wang and J. W. Rose, Film condensation in horizontal circular-section microchannels, *Proc. 5th International Symposium on Multiphase Flow, Heat Mass Transfer and Energy Conversion*, Xi'an, China, (2005).

[12] H. S. Wang and J. W. Rose, Film condensation in microchannels, *Proc. Int. Inst. Refrig. Conf. Thermophysical Properties and Transfer Processes of Refrigerants*, Vicenza, Italy. (2005) 551-558.

[13] H. S. Wang and J. W. Rose, Condensation in microchannels – effect of channel inclination, *Proc. 4th International Symposium Microchannels and Minichannels*, ASME, Limerick, Ireland, CD, paper 96049, (2006).

[14] H. S. Wang and J. W. Rose, Condensation in microchannels – comparisons of experiment and theory, *Proc. 13th International Heat Transfer Conference*, Sydney, Australia, Aug. 13-18, CD paper CSN-05, (2006).

[15] H. S. Wang and J. W. Rose, Film condensation in horizontal microchannels – effect of channel shape, *Int. J. Thermal Sciences*. 45 (2006) 1205-1212.

[16] S. Koyama, K. Kuwahara, K. Nakashita and K. Yamamoto, Condensation of refrigerant R134a in a multiport channel, *Proc. 1st Conf. on Microchannels and Minichannels*, ASME Rochester, NY. (2003) 193-205.

[17] S. Koyama, K. Kuwahara, K. Nakashita and K. Yamamoto, An experimental study on condensation of refrigerant R134a in a multiport extruded tube, *Int. J. Refrigeration*. 26 (2003) 425-432.

[18] S. W. Churchill, Friction-factor equation spans all fluid-flow regimes, *Chem. Eng.* 84 (1977) 91-92.

[19] H. S. Wang and J. W. Rose, Heat transfer during annular film condensation on microchannels: calculations for R152a, R134a, R22, R410A, propane, ammonia and carbon dioxide, *Proc. 6th Int.* Conf. on enhanced, compact and ultra compact heat exchangers, Potsdam, Germany, (2007).

[20] K. O. Beatty and D. L. Katz, Condensation of vapors on outside of finned tubes, *Chem. Eng. Prog.* 44 (1948) 55-70.

[21] H. Honda and S. Nozu, A prediction method for heat transfer during film condensation on horizontal integral-fin tubes, *Trans. ASME J. Heat Transfer*. 109 (1987) 218-225.

[22] H. Honda, H. Takamatsu and O. Makishi, Numerical analysis of film condensation on a horizontal two-dimensional fin tube, Proc. Eurotherm Seminar 47, Heat Transfer in Condensation, Paris, (1995) Elsevier 48-54.

[23] J. W. Rose, An approximate equation for the vapour-side heat-transfer coefficient for condensation on low-finned tubes, *Int J. Heat Mass Transfer*. 37 (1994) 865-875.

[24] H. S. Wang and J. W. Rose, Theoretical investigation of condensation on low-finned tubes, Proc. Heat SET 2007, Heat Transfer in Components and Systems for Sustainable Energy Technologies, Chambery, France, (2007).

[25] H. Masuda and J. W. Rose, Static configuration of liquid films on horizontal tubes with low radial fins: implications for condensation heat transfer, Proc. R. Soc. Lond. A 410 (1987) 125-139.

[26] A. Briggs, X. L. Wen and J. W. Rose, Accurate heat-transfer measurements for condensation on horizontal integral-fin tubes, *Trans. ASME, J. Heat Transfer*. 114 (1992) 719-726.

[27] A. Bella, A. Cavallini, G. A. Longo and L. Rossetto, Pure vapour condensation of refrigerants 11 and 113 on a horizontal integral-fin tube at high vapour velocity, *Enhanced Heat Transfer*. 1 (1993) 77-86.

[28] A. Cavallini, L. Dorretti, G. A. Longo and L. Rossetto, Experimental investigations on condensate flow patterns on enhanced surfaces, Proc. CFC's, The Day After, IIR Int. Conference, (1994) 627-634.

[29] A. Cavallini, L. Doretti, G. A. Longo and L. Rossetto, A new model for forced-convection condensation on integral-fin tubes, Trans. ASME J. Heat Transfer. 118 (1996) 689-693.

[30] S. Namasivayam and A. Briggs, Condensation of ethylene glycol on integral-fin tubes – effect of fin geometry and vapor velocity, Trans. ASME J. Heat Transfer. 127 (2005) 1197-1206.

[31] A. G. Michael, P. J. Marto, A. S. Wanniarachchi and J. W. Rose, Effect of vapour velocity during condensation on horizontal smooth and finned tubes, Proc. ASME Winter Annual Meeting, San Francisco, HTD 114 (1989) 1-10.

[32] S. Namasivayam and A. Briggs, Unpublished experimental data for condensation of atmospheric pressure steam on integral-fin tubes, Applied Thermal Engineering. 24 (2004) 1353-1364.

[33] S. Namasivayam and A. Briggs, Unpublished experimental data for condensation of atmosperic pressure steam on integral-fin tubes, (2005) (see Namasivayam and Briggs [35]).

[34] S. Namasivayan and A. Briggs, Unpublished experimental data for condensation of low pressure steam on integral-fin tubes, (2005) (see Namasivayan and Briggs [35]).

[35] S. Namasivayam and A. Briggs, An empirical correlation for forced-convection condensation on integral-fin tubes, Proc. 9th UK National Heat Transfer Conference, Sept., Manchester, (2005) 4-9.